SRTTU
Journal of Computational and Applied Research in Mechanical Engineering
jcarme.sru.ac.ir
JCARME
ISSN: 2228-7922

Research paper

CFD simulation and exergy evaluation of geometrical characteristics effects of refrigeration tubes in a 3-fluid LAMEE

Aydin Zabihi and Nader Pourmahmoud*

Mechanical Engineering Department, Urmia University, Urmia, Iran

Article info:

Article history:

Received: 00/00/0000
Accepted: 00/00/0018
Revised: 00/00/0000
Online: 00/00/0000

Keywords:
3-fluid LAMEE,
Refrigeration tubes,
CFD,
Exergy loss,
Effectiveness.

***Corresponding author:**
n.pormahmoud@urmia.ac.ir

Abstract

Cooling tubes are inserted into the desiccant dehumidifier liquid of a 3-fluid liquid-to-air membrane energy exchanger (LAMEE) in order to regulate the temperature of the dehumidifier liquid. As a result, the 3-fluid LAMEE's performance is significantly influenced by the refrigerated tubes. The numerical analysis of the present work shows that the number of chilled tubes and their inner diameter affect the effectiveness (total, latent, and sensible) rate of moisture removal and adequate cooling power, and exergy loss. Additionally, the dehumidifier liquid channel receives the addition of wavy cooling tubes for the first time. The relationship between wave height and wave length is known as wave steepness, and its impact on efficiency and energy loss is also examined. Numerical studies show that the number and inner diameter of the cooling tubes have a direct correlation with the efficiency of the 3-fluid LAMEE. The improved the efficiency, the more cooled tubes there are and the larger their diameter. Furthermore, both exergy loss and without dimensions exergy loss increase with the quantity and diameter of refrigerated tubes. The sensible and latent effectiveness of the 3-fluid LAMEE is increased by the wavy refrigeration tubes as compared to straight tubes; the augmentation of the sensible and latent effectiveness increases with wave steepness.

1. Introduction

Conventional methods require a substantial amount of energy to chill and remove moisture from the air. After that, liquid-to-air-membrane energy exchangers (LAMEEs) were introduced as useful devices with high efficiency. To stop the fluid streams of air and desiccant solution from merging, a membrane is placed between them in LAMEEs. To remove heat as well as moisture from the air, a dehumidifier fluid is utilized. By absorbing the heat from the air stream, the desiccant solution gets heated. Thus, the absorbing performance of the desiccant solution decreases and it needs to be regenerated. Abdel-Salam et al. [1] employed cooling tubes in the dehumidifier fluid channel to control the desiccant solution's (3-fluid LAMEE)

temperature. The researchers discovered that the 3-fluid LAMEE exhibited superior latent, total, and sensible, sensible cooling capability and moisture removal rate. The chilling of the dehumidifier liquid is, in fact, mostly dependent on the refrigeration tubes found in the 3-fluid LAMEEs. Because of this, the present article's focus is on the refrigerated tubes by examining how the quantity and inner diameter of these tubes affect the 3-fluid LAMEE's performance. The area of contact between the coolant and the dehumidifier fluid as well as the flow regime are impacted by the cooling tubes' geometry. Thus, the purpose of this work is to examine the effects of wavy tubes on the three-fluid LAMEE's efficiency and flow regime. The following summarizes previous research on dehumidification systems, 2-fluid LAMEEs, and 3-fluid LAMEEs.

In order to evaluate the fluid dehumidifier device's effectiveness during the dehumidifying and humidifying processes, Kabeel [2] conducted an experimental investigation using air injection through the calcium chloride liquid dehumidifier fluid. He investigated the desiccant solution system under various working situations such as varying temperatures, humidity ratios, and solution volumes. Liang et al. [3] suggested a novel DX (direct expansion) method that would be utilized in conjunction with a membrane-based overall heat converter in order to boost the efficiency of a typical DX system in hot and humid environments. Researchers discovered that compared to the traditional DX system, the new system's moisture removal ratio is 50% higher and its resulting ratio of efficiency is 100% larger. In another study, Storle et al. [4] evaluated and contrasted the chilling and dehydrating capacity of a pair of fluid dehumidifier membranes the air conditioning systems deployed in a hot, humid location (Miami, Florida). Their results were contrasted by looking at how latent load affected the operation of both two- and three-fluid dehumidifier membrane cooling systems. Their findings demonstrated that the 3-fluid M-LDAC system used less energy than the 2-fluid M-LDAC system. An internally-cooled parallel-plate membrane-based liquid desiccant dehumidifier (IMLDD) with ventilation tubes inside the desiccant solution channels was used in Huang et al. [5] dehumidification of air technique. They found that the IMLDD performed much better when the water input temperature was lowered to keep the temperature of the solution continuously low. A bit colder than the solution's temperature at the inlet, about 20 °C, was recommended as the water input temperature. An inventive internally-cooled supersonic combustion dehumidifying method was studied by Yang et al. [6] According to their findings, the isothermal technique was outperformed by the IC-UADS in terms of dehumidifying by an astounding 64.9%. Furthermore, if its exterior temperatures were higher than 25.6 °C, the IC-UADS might benefit from using a lower-grade cooling source, like tap water. Moreover, the ICUADS outperformed the packed-bed systems, increasing its efficiency from 47.4% to 80.1%.

Whenever deployed as an external air drier and regenerator for diluted dehumidifier liquid, Abdel-Salam et al.'s research [7] showed the sensitivity of a flat-plate LAMEE's steady-state performance to airflow and solutions channel lengths. A computational framework for combining temperature and moisture transport in a run-around heat and moisture exchanger with a liquid dehumidifier connected liquid was created by Seyed-Ahmadi et al. [8]. A run-around renewable energy system consisting of two counter-cross fluid converters functioning as regenerators and dehydrators was studied for heat transport, Vali et al. [9] built a 2-dimensional steady-state computer framework. In parallel-plate channels made of membranes, Huang et al. [10] looked into the fluid flow and convective heat mass transfer. Storle et al. [11] carried out an experimental investigation to assess the efficiency of a 3-fluid LAMEE air system for cooling. By utilizing 3-dimensional computational fluid dynamics (CFD) technology, Rashidzadeh et al. [12] modelled a 3-fluid LAMEE and looked into the process of conjugate heat and moisture transport. Using injected air through the liquid desiccant solution, Experimental research on a saltwater device using (dehumidifying and humidification) airflow was done by Kabeel et al. [13] The principles of closed-air and open-water cycles

underpin the functioning of the arrangement. Zhang [14] investigated both mass and heat exchange processes in a cross-flow parallel plate membrane enthalpy exchanger with the goal of recovering both moisture and heat from air from exhaust streams. In an experiment, the output moisture content forecast was verified. Jafarian et al. [15] offered a computational framework for fluid dehumidifier based on membranes. The model computed a more accurate boundary situation on the membrane and separating walls using the conjugate technique. They demonstrated how the model could forecast changes in the availability of air's percentage of humidity with an inaccuracy of below 3.22%. Lin et al. [16] performed a thermodynamic study on a combination membrane fluid dehumidifier dehumidifying and dehydration point evaporation cooling device. They paired a counter-flow condensation point evaporate cooler with a cross-flow membrane liquid desiccant dehumidifier.

2. The 3-fluid LAMEE model description

The 3-fluid LAMEE designed by Abdel-Salam et al.[1] had seven straight titanium refrigeration tubes (Fig. 1). The 3-fluid LAMEE with varying numbers of tubes for cooling is examined in the first half of this study (3, 4, 5, 6, 7, and 8), while the other physical properties of the refrigeration tubes such as length and thickness are kept constant. In the second section, a 3-fluid LAMEE with three refrigeration tubes are designed with the inner diameter of the refrigeration tubes varying from 1.362 mm to 2.862 mm. In the third section, wavy tubes are substituted for straight tubes, and different amounts of wave steepness are investigated from 0.3 to 1.

The other features of the 3-fluid LAMEE are equivalent to the laboratory model [1] shown in Table 1. Two 470 mm long and 2.5 mm broad air channels make up the model, and in between them is a 4.2 mm wide desiccant solution channel. Micro-porous membranes with semi-permeable properties divide the desiccant channel from the air channels to keep the flows from combining. The membranes have pores with dimensions of 30 nm and porosity of 55%, respectively. To absorb both heat and moist from the airflow, an aqueous solution of lithium chloride (LiCl) with a concentration of 32.5% flows through the desiccant solution channel. The flow pattern between the airflow and the dehumidifier fluid is counter-crossed. Conde [17] has published the properties of aqueous lithium chloride for different concentrations. Inside the refrigeration tubes, where the dehumidifier fluid is arranged in a counterflow, water flows. Fig. 2 displays a created CFD model of the 3-fluid LAMEE with seven straight chilling tubes in the current research. The geometry of the models was built with ANSYS GEOMETRY (ver. 17.2) and mesh generation of the refrigeration tubes was done by ANSYS ICEM CFD (ver. 17.2), also STAR CCM+ (Ver. 12) was applied to build the mesh of the channels for the dehumidifier liquid and airflow. The solver was ANSYS FLUENT (ver. 17.2); a finite-volume-based commercial CFD software.

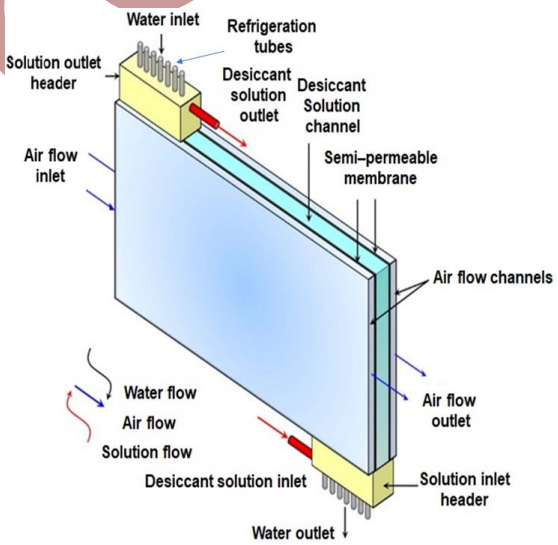

Fig.1. Diagram for the 3-fluid LAMEE[1].

Tables 1 and 2 provide summaries of the input boundary parameters and the 3-fluid LAMEE dimensions, respectively.

Table 1. Summary of the 3-fluid LAMEE specifications used for CFD model.

	Parameter	Value	Unit
Exchanger	Flow pattern (solution-air)	Counter-cross	-
	Flow pattern (refrigerant-solution)	Counter	-
	Length	470	mm
	Height	100	mm
	The aspect ratio of the exchanger (height/length)	0.31	-
	The exchanger solution entry ratio	0.11	-
	Width of the nominal air channel	5	mm
	Width of the nominal solution channel	4.2	mm
	The quantity of air channels	2	-
	Quantity of solution channels	1	-
	Mass (vacant)	1.71	kg
Membrane	Thickness	0.3	mm
	Mass resistance (R_m)	38	s/m
	Liquid pressure penetration	124	kPa
Refrigeration tubes	Refrigerant	Water	-
	Tube composition	Titanium	-
	Quantity of tubes	3, 4, 5, 6, 7, and 8	-
	Tube's length	660	mm
	Diameter inside	1.362, 1.862, 2.362, 2.862	mm
	Diameter outside	2.175, 2.675, 3.175, 3.675	mm
	Wall thickness	0.4065	mm
	Thermal conductivity	21	(W/(m·k))

$$\varepsilon_{sen} = \frac{actual\ heat\ transfer\ rate}{maximum\ possilbe\ heat\ transfer\ rate} = \frac{T_{air,in} - T_{air,out}}{T_{air,in} - T_{sol,in}} \quad (1)$$

$$\varepsilon_{lat} = \frac{actual\ moisture\ transfer\ rate}{maximum\ possible\ moisture\ transfer\ rate} = \frac{W_{air,in} - W_{air,out}}{W_{air,in} - W_{sol,in}} \quad (2)$$

$$\varepsilon_{tot} = \frac{\varepsilon_{sen} + H^* \varepsilon_{lat}}{1 + H^*} \quad (3)$$

Table 2. A list of the 3-fluid LAMEE's operating conditions.

	Input Parameter	Value	Unit
Air	Temperature, $T_{air,in}$	35.1	℃
	Humidity ratio, $W_{air.in}$	17.6	g_v/kg_{air}
	Mass flow rate	1.19	g/s
Solution	Temperature, $T_{sol,in}$	24.8	℃
	Concentration, C_{sol}	32.5	%
	Mass flow rate	0.76	g/s
Water	Temperature, $T_{w,in}$	10.1	℃
	Mass flow rate	1.98	g/s
Design and operating Parameters	NTU	1.8	-
	Cr^*	1.8	-
	Cr	0.26	-

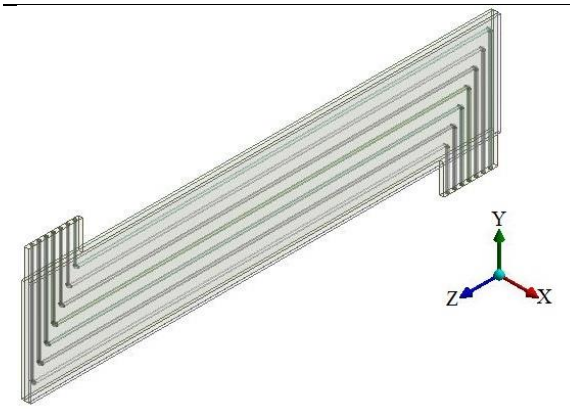

Fig. 2. CFD model of the 3-Fluid LAMEE with 7 chilling tubes.

3. LAMEEs' assessment of efficiency

Moisture removal rate ($\dot{m}_{rr}$), effectiveness (Ɛ), sensible cooling capacity (SCC), exergy loss ($\dot{E}x_{in}$), and dimensionless exergy loss (e) are important parameters to the evaluation of LAMEEs as follows:

A LAMEE can be effective in three different ways: total, sensible and latent effectiveness. Sensible effectiveness (ε_{sen}) is a proportion of realistic to maximally possible sensible heat transportation rates through the LAMEE. Latent effectiveness (ε_{lat}) is a percentage of the maximal practicable quantity of transfer of water to the real rate. Total effectiveness (ε_{tot}) is the percentage to real to the highest possible amounts of transferring energy (enthalpy). Eqs. (1-3) compute the latent effectiveness, sensible effectiveness, and overall effectiveness, as well, for a solution that can generate heat greater than the air's heat capability ($Cr^* \geq 1$).

$$\varepsilon_{sen} = \frac{actual\ heat\ transfer\ rate}{maximum\ possilbe\ heat\ transfer\ rate} = \frac{T_{air.in} - T_{air.out}}{T_{air.in} - T_{sol.in}} \quad (1)$$

$$\varepsilon_{lat} = \frac{actual\ moisture\ transfer\ rate}{maximum\ possible\ moisture\ transfer\ rate} = \frac{W_{air,in} - W_{air,out}}{W_{air,in} - W_{sol,in}} \quad (2)$$

$$\varepsilon_{tot} = \frac{\varepsilon_{sen} + H^* \varepsilon_{lat}}{1 + H^*} \quad (3)$$

Where, $T_{air.in}$ is the intake air temperature (℃), $T_{air.out}$ is the exit air temperature (℃), and $T_{sol.in}$ is the dehumidifier fluid temperature (℃) in the inlet. $W_{air.in}$ represents the entrance air humidity ratio (kg_v/kg_{air}), and $W_{air.out}$ represents the output air humidity ratio. $W_{sol.in}$ (kg/kg) is the balanced ratio of humidity of the incoming saline liquid. Additionally, Eq. (4) can be used to derive H*, which is the operational factor [18].

$$H^* = \frac{\Delta H_{lat}}{\Delta H_{sen}} \approx 2500 \frac{W_{air.in} - W_{sol.in}}{T_{air.in} - T_{sol.in}} \quad (4)$$

The effectiveness of transfer of moisture and heat amongst the airflow and the dehumidifier liquid in 3-fluid LAMEEs can be assessed using the conventional effectiveness equations (Eqs. (1-3)). In specific operational circumstances, this effectiveness is higher than 100% (high mass flow rates of cooling water at low inlet temperatures) [1,12,19], which is in opposition to the equations describing the physical effectiveness of energy exchangers. Therefore, Abdel-Salam et al. [19] altered the traditional effectiveness equations for 3-fluid LAMEE and presented the following total effectiveness equations:

$$\varepsilon_{sen} = \frac{T_{air,in} - T_{air,out}}{T_{air,in} - T_{ref,in}} \quad (5)$$

$$\varepsilon_{lat} = \frac{W_{air,in} - W_{air,out}}{W_{air,in} - W_{sol,in@C_{sol,in}\&T_{ref,in}}} \quad (6)$$

Where $W_{sol.in@C_{sol.in}\&T_{ref.in}}$ the comparable ratio of humidity of the inlet dehumidifier fluid, is calculated at the inlet coolant temp (g/kg) and the inlet dehumidifier fluid saturation.

According to Eq. (7), the moisture removal rate (being the rate at which moisture is moved from the streams of dehumidifier fluid to the airflow) is another crucial factor in determining how well a LAMEE performs.

$$\dot{m}_{rr} = \dot{m}_{air} |W_{air,out} - W_{air,in}| \quad (7)$$

Where $\dot{m}_{air}$ is the mass flow rate of the inlet air (kg/s).

The cooling capacities of a LAMEE are determined by the quantity of heat exchange through the streams of airflow and dehumidifier fluid.

$$SCC = \dot{m}_{air} c_{p,air} (T_{air,in} - T_{air,out}) \quad (8)$$

Where $c_{p.air}$ represents the air's particular thermal capability (J/kg. K).

The number of heat transfer units (NTU) significantly affect a LAMEE's practical effectiveness [1,20].

$$NTU = \frac{UA}{C_{min}} \quad (9)$$

$$U = \left[\frac{1}{h_{air}} + \frac{\delta}{k_{mem}} + \frac{1}{h_{sol}}\right]^{-1} \quad (10)$$

In this case, δ is the membrane's width (m), k_{mem} is the membrane thermal efficiency (W/m.K), h_{air} is the conduction heat transfer

factor of the airflow($W/m^2.K$), A is the area of the membrane's surface (m^2), C_{min} is the lowest thermal conductivity rate of the airflow and dehumidifier fluid streams (W/K), h_{sol} the convection heat transmit ratio of the dehumidifier fluid (W/m.K), and U is the overall heat transfer coefficient (W/m^2K).

A LAMEE's latent efficiency is determined by its total mass transfers unit (NTUm) count, which is determined by the following definition:

$$NTU_m = \frac{U_m A}{\dot{m}_{min}} \quad (11)$$

$$U_m = [\frac{1}{h_{m,air}} + \frac{\delta}{k_m}]^{-1} \quad (12)$$

In this equation, U_m denotes the total coefficient of mass transfer (kg/m^2 s), $\dot{m}_{min}$ denotes the lowest mass flow rate of the airflow and dehumidifier fluid (kg/s), $h_{m.air}$ represents the convection mass transfer ratio of the airflow(kg/m2 s), $h_{m.sol}$ represents the conduction mass transfer ratio of the dehumidifier fluid (kg/m2 s), and k_m indicates the water permeation of the membrane's surface (kg/m s) [21].

The relationship of the heat capability rates for the dehumidifier fluid to the airflows is expressed as Cr^*. The relationship of the dehumidifier and the letter Cr stands for the lowest and highest heat capacity amounts of coolant fluids.

$$Cr^* = \frac{C_{sol}}{C_{air}} = \frac{\dot{m}_{sol}\, c_{p.sol}}{\dot{m}_{air} c_{p.air}} \quad (13)$$

$$Cr = \frac{C_{min}}{C_{max}} = \frac{C_{sol}}{C_{ref}} = \frac{\dot{m}_{sol}\, c_{p.sol}}{\dot{m}_{ref} c_{p.ref}} \quad (14)$$

$C_{p\,air}$ represents the particular heat capacity of the airflow, $C_{p\,ref}$ is the particular heat capacity of the coolant, $C_{p\,sol}$ and is the particular heat capacity of the dehumidifier liquid (j/kg. k). The mass flow rate of the solution is expressed as $\dot{m}_{sol}$ (kg/s), and the mass flow rate of the cooling fluid is expressed as $\dot{m}_{ref}$ (kg/s).

The ratio of dehumidifier mass to water solution is known as the concentration of dehumidifier fluid.

$$C_{sol.in} = \frac{\text{mass of desiccant}}{\text{mass of desiccant+mass of water}} \quad (15)$$

4. Developing formulas

The 3-Fluid LAMEE is expected to include a 3-dimensional framework for laminar and steady state flows. The following are the basic equations that govern the dynamics of fluid flow. The following formula describes mass conservation, often known as continuity:

$$\frac{\partial \rho}{\rho t} + \nabla \cdot (\rho \vec{v}) = S_m \quad (16)$$

S_m consists of any user-defined sources and the mass contributed to the continuous phase by the dispersed second phase (e.g., condensate transfer via the membrane).

$$\frac{\partial}{\partial t}(\rho \vec{v}) + \nabla \cdot (\rho \vec{v}\vec{v}) = -\nabla p + \nabla \cdot (\bar{\bar{\tau}}) + \rho \vec{g} + \vec{F} \quad (17)$$

The formula for momentum is found in Eq. (17), when the exterior body force is represented by $\vec{F}$ and the gravitation mass force by $\rho \vec{g}$ ⃗ and $\bar{\bar{\tau}}$ is the stress tensor and the gravitation mass force by P, additional model-dependent resource concepts, like porous-media and user-defined sources, are covered as well in $\vec{F}$. The energy formula is solved by ANSYS Fluent in the manner shown below:

$$\frac{\partial}{\partial t}(\rho E) + \nabla \cdot \left(\vec{v}(\rho E + p)\right) = \nabla \cdot \left(K_{eff} \nabla T - \sum_j h_j \vec{j}_j + (\bar{\bar{\tau}}_{eff} \cdot \vec{v})\right) + S_h \quad (18)$$

K_{eff} stands for effective conductivity, and $\vec{j}_j$ is the species j diffusion flux. Energy transfer resulting from conduction, species diffusion, and viscous dissipation are each represented by the first three terms on the right. Also, $E = h - \frac{p}{\rho} + \frac{v^2}{2}$ and $h = \sum_j Y_j h_j$.

The primary challenge in the computational fluid dynamics (CFD) modelling of the current efficiency converter is resolving the extra formulas for thermal and humidity transfer among the dehumidifier fluid and the humid airflow. Because computation is greatly impacted by the presence of a membrane that is partially permeable with specific characteristics

like width, pores, and permeability. The steps involved in this process are as follows: (1) transferring moist from the airflow to the dehumidifier fluid; (2) transport of heat between two fluids at the membrane- dehumidifier fluid contact; and (3) expulsion of heat as a result of the phase change of the conveyed water vapor inside the dehumidifier fluid. In addition, the previously listed components must include the capture of both the diffusion and the absorption processes [9,22,23]. Water vapor and the utilization of the rule of conservation of mass:

$$\frac{2U_m y_0}{m_{air}}(W_{air} - W_{sol}) = -\frac{\partial W_{air}}{\partial x} \quad (19)$$

The humidification ratio of the airflow, or the ratio of the amount of water vapor in the airflow to the mass of without moisture, is represented by the formula $W_{air} = \frac{\text{mass } H_2O}{\text{mass Air}} = f(\emptyset_{air}. T_{air})$ and is dependent on both the temperature and the relative humidity. U_m stands for the total mass transfer coefficient. Moreover, W_{sol}, a function of the concentration of solution and temperature, is the humidity ratio of air in agreement with the salt liquid; $W_{sol} = f(X_{sol}. T_{sol})$. Hemingson et al. [21] have shown that humidity transfer friction on the dehumidifier side is minimal, resulting in $W_{sol} \approx W_{sol,membrane}$. On the liquid side, mass conservation of water can be taken into account:

$$2U_m(W_{air} - W_{sol}) = \rho_{salt} d_{sol}(u_{sol}\frac{\partial X_{sol}}{\partial x} + v_{sol}\frac{\partial X_{sol}}{\partial y}) \quad (20)$$

Where X_{sol} represents the mass of water in salt solution as a percentage of the total mass of salt; $X_{sol} = \frac{\text{Mass } H_2O}{\text{Mass Pure Salt}}$. The equation for energy conservation on the air side is as follows:

$$\frac{2Uy_0}{C_{air}}(T_{air} - T_{sol}) = -\frac{\partial T_{air}}{\partial x} \quad (21)$$

Where $C_{air} = \dot{m}_{air}\, c_{p.air}$, and U represents the heat transfer coefficient total. Related saving energy on the fluid portion is:

$$2U(T_{air} - T_{sol}) + 2U_m h_{fg}(W_{air} - W_{sol}) = (\rho c_p d)_{sol}(u_{sol}\frac{\partial T_{sol}}{\partial x} + v_{sol}\frac{\partial T_{sol}}{\partial y}) \quad (22)$$

Here, $2U_m h_{fg}(W_{air} - W_{sol})$ is the energy released as a result of the water's phase shift. The three-fluid LAMEE's heat and moisture transport processes are modelled using the additional set of Eqs. (19–22). There is no easy way to tackle these in the ANSYS FLUENT software. These equations are resolved using external programming languages called UDS (User Defined Scalar).

4.1. Exergy loss analysis

The most productive labor that can be produced by a reversible process is called energy. For a constant control volume, the exergy balance can be expressed as follows:

$$\sum \dot{E}x_{in} - \sum \dot{E}x_{out} + \sum \dot{E}x_{product} = 0 \quad (23)$$

The discrepancy between maximal effort and actual work is known as energy loss:

$$\dot{E}x_{loss} = \dot{W}_{max} - \dot{W}_{actual} \quad (24)$$

For a three-fluid LAMEE, the expression for energy loss in an adiabatic stable system with three distinct kinds of working fluids is as follows:

$$\dot{E}x_{loss} = \dot{E}x_{loss\ air} + \dot{E}x_{loss\ sol} + \dot{E}x_{loss\ ref} \quad (25)$$

Where $\dot{E}x_{loss\ air}$, $\dot{E}x_{loss\ sol}$, and $\dot{E}x_{loss\ ref}$ are exergy loss for air, solution, and refrigerant streams respectively, which can be calculated from the following equations [24]:

$$\dot{E}x_{loss\ air} = T_e[\dot{m}_{air}(s_{air\ out} - s_{air\ in})] \quad (26)$$

$$\dot{E}x_{loss\ sol} = T_e[\dot{m}_{sol}(s_{sol\ out} - s_{sol\ in})] \quad (27)$$

$$\dot{E}x_{loss\ ref} = T_e[\dot{m}_{ref}(s_{ref\ out} - s_{ref\ in})] \quad (28)$$

The following is an expression for entropy gradients in terms of particular temperatures under a steady pressure. [25,26]:

$$s_{air\ out} - s_{air\ in} = c_{p\ air} \ln\left(\frac{T_{air\ out}}{T_{air\ in}}\right) \quad (29)$$

$$s_{sol\ out} - s_{sol\ in} = c_{p\ sol} \ln\left(\frac{T_{sol\ out}}{T_{sol\ in}}\right) \quad (30)$$

$$s_{ref\ out} - s_{ref\ in} = c_{p\ ref} \ln\left(\frac{T_{ref\ out}}{T_{ref\ in}}\right) \quad (31)$$

Substituting Eqs. (29-31) into Eqs. (25-28) yields:

$$\dot{E}x_{loss} = T_e \left[\dot{m}_{air} c_{p\,air} \ln\left(\frac{T_{air\,out}}{T_{air\,in}}\right) + \dot{m}_{sol} c_{p\,sol} \ln\left(\frac{T_{sol\,out}}{T_{sol\,in}}\right) + \dot{m}_{ref} c_{p\,ref} \ln\left(\frac{T_{ref\,out}}{T_{ref\,in}}\right)\right] \quad (32)$$

From Eq. (33) one can derive the dimensionless exergy loss (e).

$$e = \frac{\dot{E}x_{loss}}{T_e C_{min}} \quad (33)$$

Where $C_{min} = \min\{C_{air} = \dot{m}_{air} c_{p\,air}. C_{sol} = \dot{m}_{sol} c_{p\,sol}. and\ C_{ref} = \dot{m}_{ref} c_{p\,ref}\}$.

5. Numerical Details

Fig. 3 displays the mesh customized for the computational domain. To ensure the mesh formation process, the 3-fluid LAMEE is subjected to mesh independence tests using three straight refrigeration tubes and inlet water at 10.1 °C and Cr=0.26. The relative errors of the calculated outlet air temperature (°C) and outlet air humidity ratio (g_v/kg_{air}) as the main criteria are less than 2% as a result of gradually reducing the mesh size. According to the number of 7 tubes and their thickness, as well as the air channels, membranes and solution channel, all these objects have been meshed separately in STAR-CCM+ software to reduce the number of meshes and assembled inside Ansys Fluent. Consequently, a domain with 2403043 items was chosen.

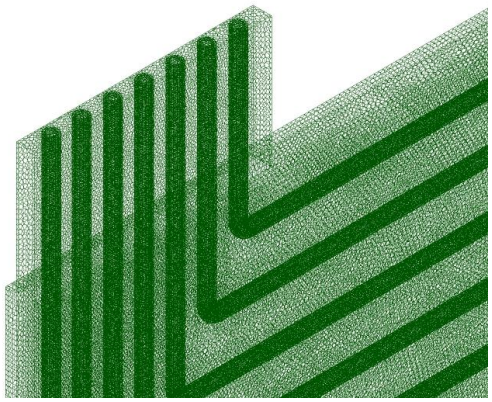

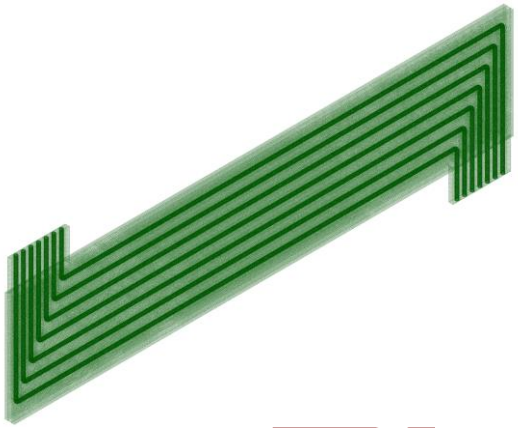

Fig. 3. 3-fluid LAMEE grid system.

To validate the numerical model and computational methods, the sensible and latent effectiveness of the current CFD findings is compared with the experimental data [1]. Different temperatures of the inlet water from 10.1 °C to 24.6 °C are tested for a 3-fluid LAMEE with seven refrigeration tubes meanwhile the heat capacity ratio (Cr) is 0.26. The geometry and operating conditions are similar to the experimental case as mentioned in Tables 1 and 2. As shown in Fig. 4, both latent and sensible effectiveness show good agreements. The greatest deviation of the latent effectiveness is approximately 7%, whereas the variation of the sensible effectiveness is within 8%, indicating the high fidelity of the mathematical framework and methodologies employed in this work.

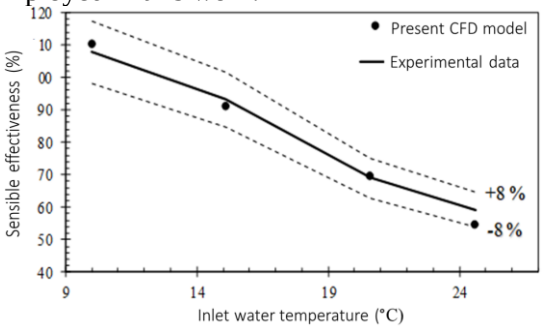

(a)

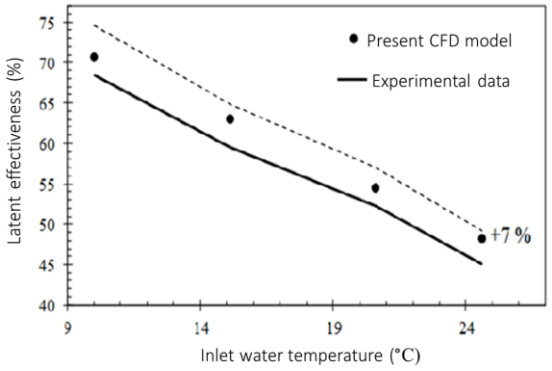

(b)

Fig. 4. Comparison of the numerical results of the present study with experimental data (a) sensible effectiveness, (b) latent effectiveness.

6. Results and discussions

To regulate the desiccant's temperature, refrigeration tubes are inserted into the desiccant solution channel. Thus, the 3-fluid LAMEE's performance is greatly impacted by the refrigerated tubes' cooling capacity. The three most significant design factors of the refrigeration tubes that are examined in this work are their number, diameter, and form.

6.1. The impact of the quantity of cooling tubes

The influence of the quantity of cooling tubes (3, 4, 5, 6, 7, and 8) on the efficiency of the 3-fluid LAMEE is explored in this section, and the traditional and overall efficacy in proportion to the number of refrigerated tubes are shown in Fig. 5.

One may generally conclude that the quantity of cooled tubes and effectiveness are directly correlated, and that all forms of effectiveness rise with the number of refrigeration tubes. Because there are more tubes in the traditional sensible effectiveness, its slope is steeper than the latent effectiveness's. When the quantity of cooling tubes exceeds five tubes, the amount of traditional sensible effectiveness becomes more than 100%. The slope of the sensible effectiveness is steeper than the slope of the latent effectiveness in Fig. 5 (b), but for different number of tubes, both the sensible and latent effectiveness are less than 100%. When the number of tubes is fewer than six, the overall latent effectiveness is more than the sensible effectiveness; but when the number of tubes is six or seven, they are roughly equal. Furthermore, as the number of tubes exceed seven, the overall sensible effectiveness exceeds the overall latent effectiveness. The most effective dryer has been designed with internal cooling, as demonstrated by Jafarian et al. [15].

The improvement in effectiveness with increasing the number of tubes is described as follows: According to Table 1, the length and outer diameter of a tube are 660 mm and 3.175 mm respectively, resulting in a contact surface area of 6579.87 mm2 with the desiccant. According to Table 3, there is a direct relationship between the number of tubes and the surface area where the desiccant solution and refrigerant stream come into contact. The conductive and conductive heat transfer between the desiccant and refrigerant (water) rises as the contact surface area increases.

Consequently, the dehydrating solution's temperature drops, increasing the temperature differential that exists among the dehumidifier and airflow streams, which in turn increases heat transfer between two sides (raising sensible effectiveness (Eq. (1)), and boosting refrigeration tube chilling capacity. The desiccant temperature reduction causes the desiccant vapor pressure to decrease, which in turn causes the vapor pressure difference among dehumidifier and airflow to increase (as a possibility for moist transport). Therefore, the latent effectiveness increases with the increase of the moisture transfer. As a result, moisture transfer and latent effectiveness both rises. According to Eq. (3), total effectiveness is dependent on sensible and latent effectiveness, and total effectiveness increases with the increase in the number of tubes.

Table 3. The impact of the quantity of tubes on the overall contact region.

Number of tubes	Total contact surface area (mm^2)
3	19739.6
4	26319.5
5	32899.4
6	39479.2
7	46059.1
8	52639.0

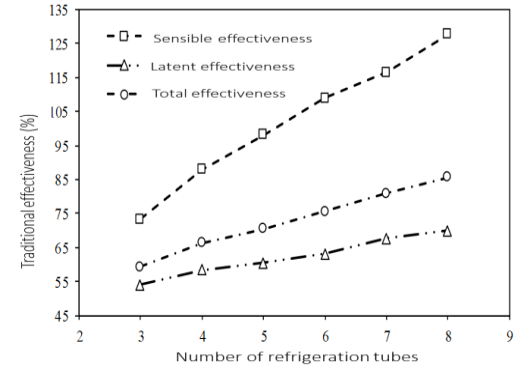

(a)

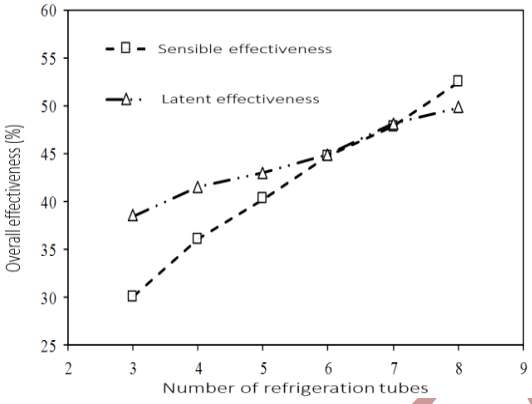

(b)

Fig. 5. The impact of the number of cooling tubes on (a) traditional effectiveness and (b) overall effectiveness.

Fig. 6 shows how the number of tubes affects the sensible cooling capacity and moisture removal rate. Both of them increase as the number of refrigerated tubes increase. Because as the quantity of cooling tubes rises, the heat transfer (sensible cooling capacity) and moisture transfer (moisture removal rate) from the air side to the desiccant side rises as well. Therefore, the temperature and humidity ratio of the air decrease at the outlet of the 3-fluid LAMEE. According to Table 2, the humidity ratio and temperature of the inlet air are 17.6 g_v/kg_{air}, 35.1 °C respectively ($W_{air\ in}$= 17.6 g_v/kg_{air}, $T_{air\ in}$= 35.1 °C). Table 4 shows the reduction of the humidity ratio and temperature of the air stream (at outlet) in the 3-fluid LAMEE with the different number of tubes.

Table 4. The effect of the number of tubes on the humidity ratio and temperature of the air.

Number of tubes	Decrease of the air humidity ratio (%)	Decrease of the air temperature (%)
3	34.1	2.4
4	36.8	2.9
5	38.1	3.3
6	39.8	3.6
7	42.6	3.9
8	44.1	4.3

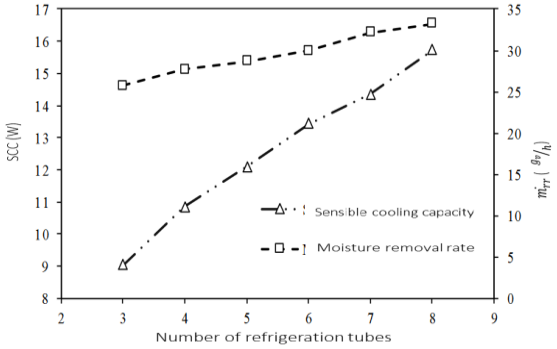

Fig. 6. The effect of the number of the cooling tubes on the sensible cooling capacity and moisture removal rate.

Fig. 7 depicts the influence of tube number on exergy loss and dimensionless exergy loss. The quantity of exergy loss rises as the quantity of cooling tubes grows. The largest and least exergy loss occur in the 3-fluid LAMEE with eight and three cooling tubes, respectively. The irreversibility of the 3-fluid LAMEE is due to losses of the heat and moisture transfer and the frictional pressure drop. As mentioned above, the heat and moisture transfer increase as the number of the refrigeration tubes increases, therefore the exergy loss owning to heat and moisture transfer irreversibility increases. Besides, the frictional pressure drop of the system (especially in the desiccant solution channel) increases with the increase of the tubes number.

As a result, the exergy loss of the 3-fluid LAMEE increases as the tubes number increases. The exergy loss increases at about 6% on average with increasing one refrigeration tube. For example, the amount of the exergy loss increases from 53.5 (W) to 56.8 (W) as the tubes

number increases from six to seven. The relationship between the dimensionless exergy loss (e) and the tubes number is shown in Fig. 7(b). The dimensionless exergy loss increases with the increase in the number of tubes.

The dimensionless exergy loss (e) depends on both of the exergy loss ($\dot{E}x_{loss}$) and C_{min} (see Eq. (26)). Since the inlet mass flow rates and temperatures are constant for different cases, the value of C_{min} is constant ($C_{min}=C_{air}=1.2$ W/K). Therefore, there is a direct relationship between the exergy loss and dimensionless exergy loss.

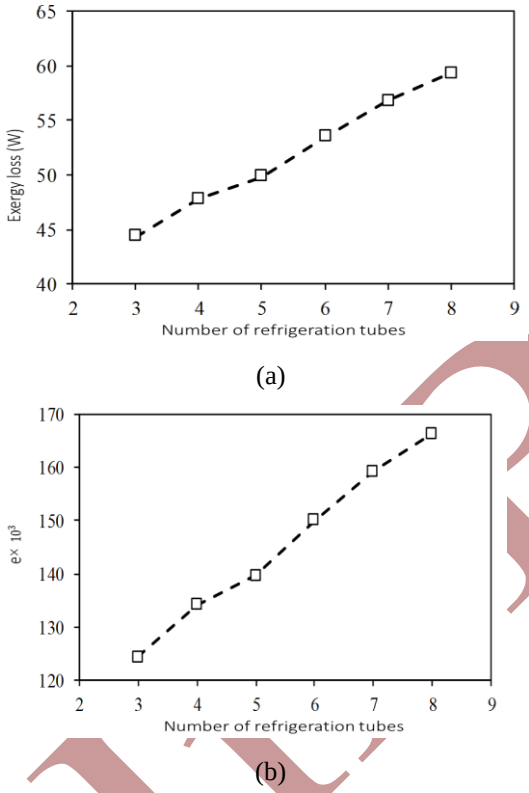

Fig. 7. The effect of the number of the refrigeration tubes on the (a) exergy loss, and (b) dimensionless exergy loss.

6.2. Effect of diameter of the refrigeration tubes

Since the diameter of the refrigerated tubes has a considerable influence on the cooling capacity of the refrigerant, in this section, the effect of the tube diameter on the effectiveness, sensible cooling capacity, moisture removal rate, and exergy loss is researched. A 3-fluid LAMEE including three refrigeration tubes is investigated with different inner diameters of the refrigeration tubes (1.362, 1.862, 2.362, and 2.862 mm) and the other design parameters such as thickness and length of the tubes are kept constant. Higher tubes diameters are impossible due to the restriction of the width of the desiccant solution channel.

Fig. 8 depicts the effect of tube widths on traditional and overall effectiveness. As the diameter of the tube increases, its traditional and overall effectiveness increases as well. For both the traditional and overall techniques, the sensible effectiveness slope is steeper than the latent effectiveness. As a result, it is possible to deduce that increasing the tube width has more influence on sensible effectiveness than latent effectiveness. For example, as the inner diameter of the tubes increases from 1.362 mm to 2.862 mm, the traditional sensible effectiveness improves by 2.2%, while the traditional latent effectiveness increases by 0.5%. Traditional sensible effectiveness numbers are more than latent effectiveness for each tube diameter, but for the overall approach, latent effectiveness is higher than sensible effectiveness for varied tube diameters.

Compared to the standard effectiveness equations utilized in the literature, Abdel-Salam et al. [19] demonstrate that the overall performance criteria yield effectiveness values that are less sensitive to variations in the inlet refrigerant temperature and, therefore, are more appropriate for energy exchanger design.

Table 5 shows the total contact surface areas between the desiccant solution and the refrigerant for various refrigeration tube inner diameters. The total contact area improves as the tube's diameter rises. As previously stated, increasing contact surface area improves the potential for the transfer of moisture and heat (with temperatures ranging and pressure of vapor differential among airflow and dehumidifier flows). As a result, as the inner diameter of the refrigerated tubes increases, the total, sensible, and sensible effectiveness also grow. Furthermore, as the diameter of the cooling tubes grows, the refrigerant velocity decreases, while the mass flow rate of the tubes remains constant. As a result, the refrigerant's residence time in the refrigeration tubes increases, allowing the refrigerant to obtain

greater heat transfer from the dehumidifier fluid and better control the temperature of the dehumidifier fluid.

Table 5. The effect of the diameter of the tube on the total contact surface area.

Inner diameter of tubes (mm)	Total contact surface area (mm^2)
1.362	13522.4
1.862	16631.0
2.362	19739.6
2.862	22848.2

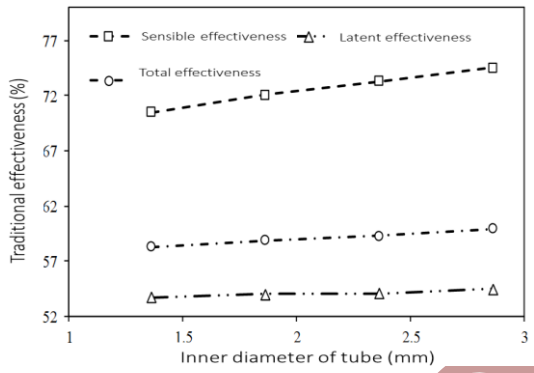

(a)

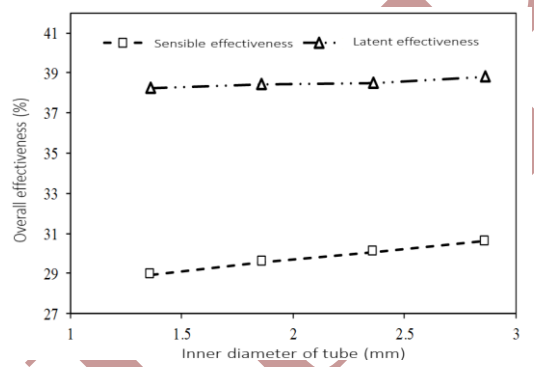

(b)

Fig. 8. The effect of the diameter of the cooling tubes on the (a) traditional effectiveness, (b) overall effectiveness.

The reasonable cooling capacity and moisture removal rate are plotted against the inner diameter of the refrigerated tubes in Fig. 9. The sensible cooling capacity increases roughly linearly with the increase of the tubes diameter, but the slope of the moisture removal rate curve varies as the tubes diameter grows.

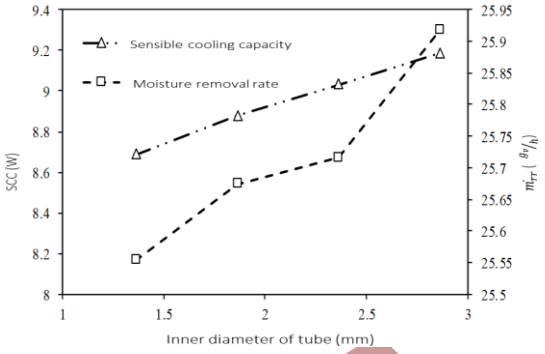

Fig. 9. Variations of the sensible cooling capacity and moisture removal rate with the inner diameter of the refrigeration tubes.

The variations of the exergy loss ($\dot{E}x_{loss}$) and dimensionless exergy loss (e) are illustrated in Fig. 10. The exergy loss increases with the increase in the diameter of the tubes. For example, the exergy loss increases 1% as the inner diameter of the tubes increases from 1.362 mm to 1.862 mm. As mentioned above, there is a direct relationship between the exergy loss and dimensionless exergy loss. Therefore, the dimensionless exergy loss increases as the diameter of the refrigeration tubes increases. With the increase in the diameter of the tube: (1) the heat transfer from the desiccant solution to the refrigerant increases, (2) the heat and moisture transfer from the air stream to the desiccant solution stream increase. Consequently, more heat and moisture transfer cause more irreversibility and more exergy loss.

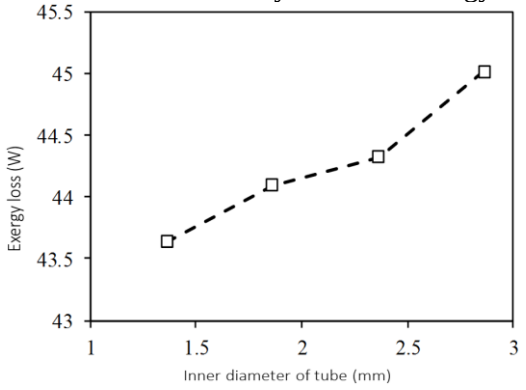

(a)

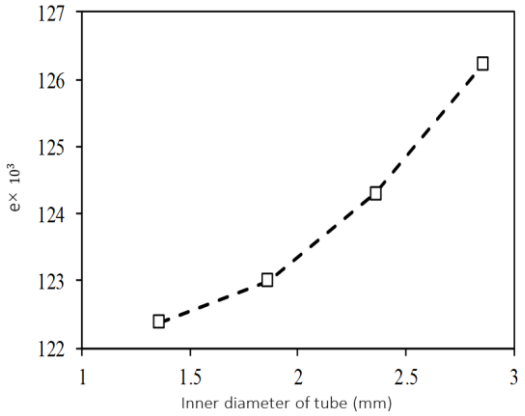

(b)

Fig. 10. The effect of the diameter of the refrigeration tubes on the (a) exergy loss, and (b) dimensionless exergy loss.

6.3. The influence of wavy refrigeration tubes

The shape of the cooling tubes is one of the most significant parameters on the performance of the 3-fluid LMAEE. Thus, in this section the influence of the shape of tubes is studied. Wavy tubes are being investigated to improve the ability to cool of cooling tubes. Fig. 11 depicts a 3-fluid LAMEE with three wavy cooling tubes.

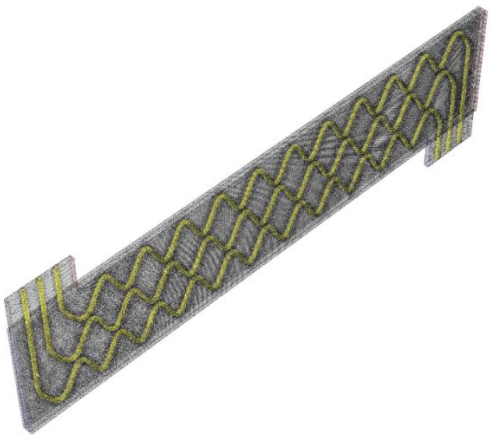

Fig. 11. 3-fluid LAMEE with three wavy refrigeration tubes.

A wave is defined with two parameters, namely as length and height of the wave (see Fig. 12). The ratio between the wave height and wave length is introduced as wave steepness.

$$\text{wave steepness} = \frac{\text{wave height}}{\text{wave length}} \tag{33}$$

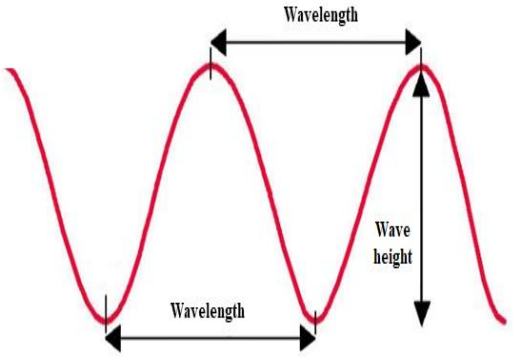

Fig. 12. A schematic of a wave with two characteristics.

The present research investigates the effects of wave steepness on 3-fluid LAMEE efficiency. The waves height is kept fix (24 mm) due to the restriction of the channel height, and the waves length is changed from 24 mm to 72 mm.

The sensible and latent effectiveness (traditional and total) of the three-fluid LAMEE with three straight refrigeration tubes and the three-fluid LAMEE with three wavy refrigeration tubes are compared in Fig. 13. It is obvious that wavy refrigerated tubes improve both the sensible and latent efficacy of the 3-fluid LAMEE as compared to straight tubes, and the improvement increases by the increase in wave steepness. For instance, overall sensible effectiveness increases from 30.1% to 31.2% and 36.5%, respectively, in comparison to the 3-fluid LAMEE with straight tubes, while total latent effectiveness increases from 38.5% to 39.3% and 41.8%.

Relatively short liquid flows outlet and inlet distances and a low converter ratio of aspect yield the maximum total sensible efficacy for an identified total dimension of the converters [9].

The improved sensible and latent efficacy of the 3-fluid LAMEE with wavy refrigeration tubes is explained as follows: (1) The interaction region (approximate the coolant and dehumidifier fluid) is increased when wavy cooling tubes are added to the 3-fluid LAMEE. The capacity of the cooled tubes to regulate temperature is directly

correlated with their interaction with region, as was previously mentioned. (2) As shown in Fig. 14 (a) , the stream lines of the desiccant flow change depending on the shape of the refrigeration tubes, and the flow regime changes from laminar to turbulent when wavy refrigeration tubes are used, which in turn increase the desiccant solution's convective and conductive heat transfer coefficients. Fig. 14(b) makes it evident how the wavy cooling tubes affect the dehumidifier fluid flow's chilling. (3) The residence period of the dehumidifier fluid and chiller in the 3-fluid LAMEE rises, giving them more time to heat exchange. As a result, the temperature of the desiccant solution decreases, and the temperature and vapor pressure differential between the air and the desiccant solution increase (as the potentials for heat and moisture transfer increase). The three cited reasons cause the increase in the wave steepness. Therefore, the sensible and latent effectiveness grow as the wave steepness grows.

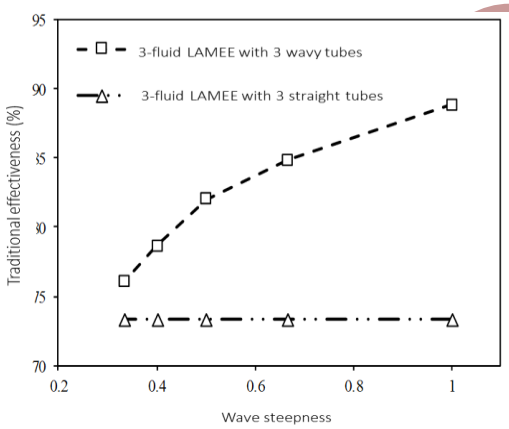

(a)

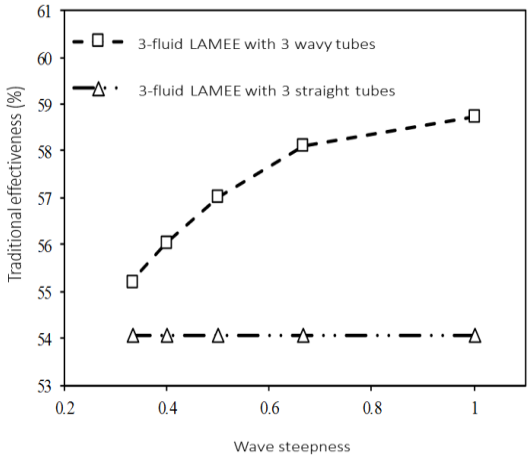

(b)

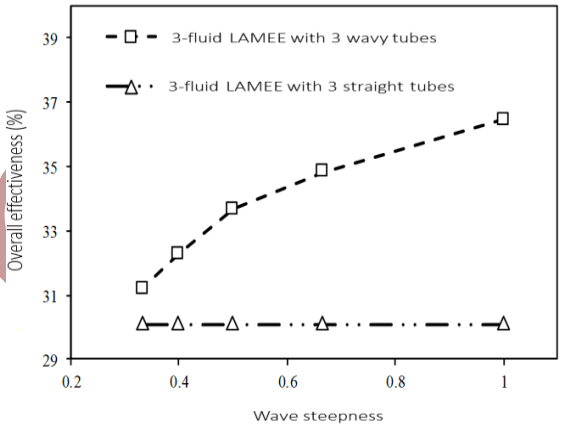

(c)

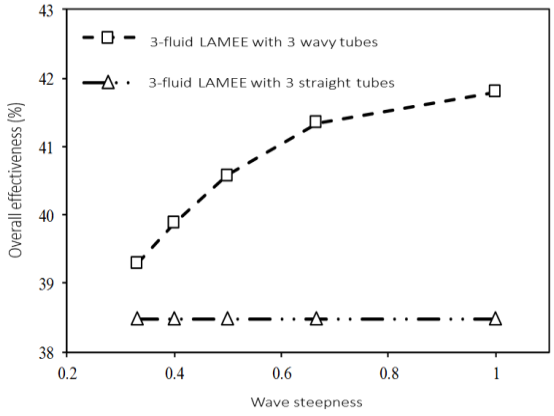

(d)

Fig. 13. The effect of the wave steepness on the (a) traditional sensible effectiveness, (b) traditional latent effectiveness, (c) overall sensible effectiveness, and (d) overall latent effectiveness with wavy refrigeration tubes and the 3-fluid LAMEE with straight tubes.

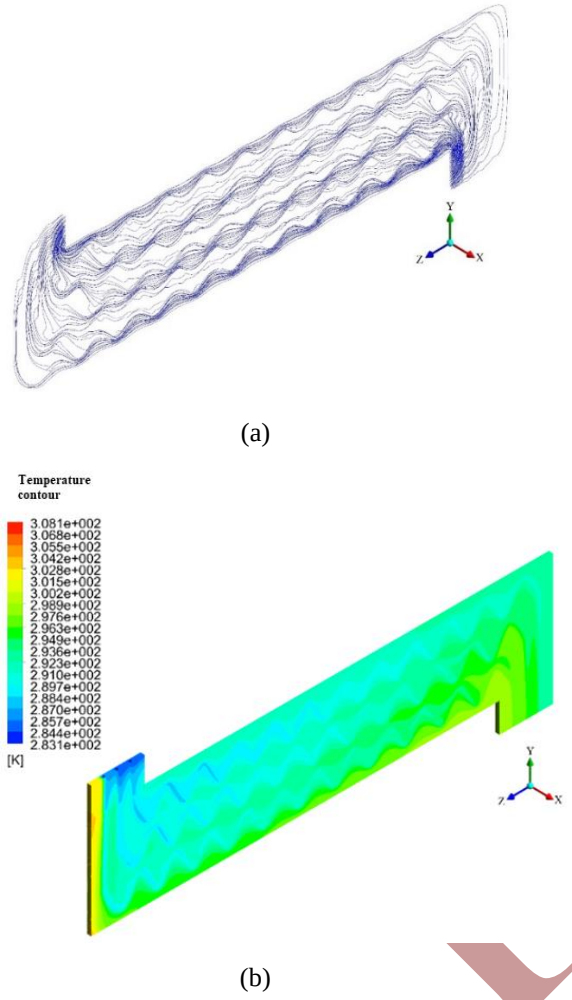

(a)

(b)

Fig. 14. (a) Streamlines of the dehumidifier fluid, (b) temperature contour of the dehumidifier fluid stream.

Fig. 15 shows a comparison between the exergy loss ($\dot{E}x_{loss}$) and dimensionless exergy loss (e) of the 3-fluid LAMEE with three straight refrigeration tubes as well as the 3-fluid LAMEE with wavy cooling tubes at various wave steepness. The wavy refrigeration tubes increase both exergy loss and dimensionless exergy loss of the 3-fluid LAMEE. Besides, the exergy loss and dimensionless exergy loss increase as the wave steepness increases.

As explained above, the wavy refrigeration tubes increase the heat and moisture transfer, therefore the exergy loss due to heat and moisture transfer irreversibility increases with the increase of the wave steepness. In addition, the frictional pressure drops of the dehumidifier fluid and waterflow increase as the wave steepness increases. Therefore, more frictional pressure drop causes more irreversibility and more exergy loss.

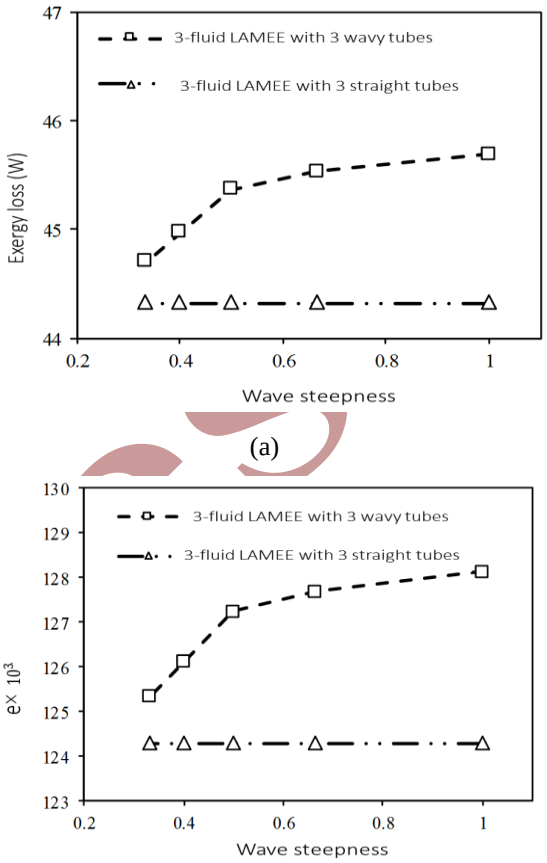

Fig. 15. The effect of the wavy refrigeration tubes on the (a) exergy loss, and (b) dimensionless exergy loss.

7. Conclusions

This study investigated the effects of the number and inner diameter of the refrigerated tubes on the effectiveness (sensible, latent, and total), moisture removal rate, sensible chilling capacity, exergy loss, and dimensionless exergy loss. Also, the wavy cooling tubes used inside the dehumidifier fluid channel and the effect of the wave steepness on the effectiveness and exergy loss is studied as well. From the results of the present study, the following main conclusions can be drawn:

1. The potential for heat and moisture transfer between air flows and solution

desiccant increases due to the direct relationship between the number of tubes and the contact surface area of the absorbent dehumidifier fluid and water. As the quantity of cooling tubes increases, the cooling capacity of tubes increases and the temperature of the absorbent solution decreases, which in turn increases the potential for these two factors to occur.

2. Increasing the diameter of the cooling tubes increases the latent, total, and sensible effectiveness and also increases the sensible chilling capacity and dehumidification rate.

3. Irreversibility caused by heat and moisture transfer and frictional pressure drop increase by increasing the number of tubes and increasing the diameter of the tubes, which leads to an increase in exergy loss.

4. The length of the tube in the absorbent solution channel is extended in absorption membrane energy converters with corrugated tubes. And because of their wavy shape, the flow regime changes from laminar to turbulent, increasing the transfer of displacement heat and conductivity between the solution desiccant flow and water flow. Additionally, the temperature of the desiccant is better controlled, which ultimately improves system efficiency.

References:

[1] M.R. Abdel-Salam, R.W. Besant, C.J. Simonson, "Design and testing of a novel 3-fluid liquid-to-air membrane energy exchanger (3-fluid LAMEE) ", *Int. J. Heat Mass Transf.*, Vol.92, No.pp.312-329,(2016).

[2] A. Kabeel, "Dehumidification and humidification process of desiccant solution by air injection", *Energy.*, Vol. 35, No. 12, pp. 5192-5201, (2010).

[3] C. Liang, L. Zhang, L. Pei, "Performance analysis of a direct expansion air dehumidi fi cation system combined with membrane-based total heat recovery", *Energy.*, Vol. 35, No. 9, pp. 3891-3901, (2010).

[4] D. Storle, M.R. Abdel-Salam, C.J. Simonson, "Energy performance comparison of a 3-fluid and 2-fluid liquid desiccant membrane air-conditioning systems in an office building", *Energy.*, Vol. 176, No. pp. 437-456, (2019).

[5] S-M. Huang, M. Yang, B. Hu, S. Tao, F.G Qin, W. Weng, et al, "Performance analysis of an internally-cooled plate membrane liquid desiccant dehumidifier (IMLDD): An analytical solution approach", *Int. J. Heat Mass Transf.*, Vol. 119, No. pp. 577-585, (2018).

[6] Z. Yang, R. Tao, H. Ni, K. Zhong, Z. Lian, "Performance study of the internally-cooled ultrasonic atomization liquid desiccant dehumidification system", *Energy.*, Vol. 175, No. pp. 745-757,(2019).

[7] M.R. Abdel-Salam, R.W. Besant, C.J. Simonson, "Sensitivity of the performance of a flat-plate liquid-to-air membrane energy exchanger (LAMEE) to the air and solution channel widths and flow maldistribution", *Int. J. Heat Mass Transf.*, Vol. 84, No. pp. 1082-1100, (2015).

[8] M. Seyed-Ahmadi, B. Erb, C.J. Simonson, R.W. Besant, "Transient behavior of run-around heat and moisture exchanger system. Part I: Model formulation and verification", *Int. J. Heat Mass Transf.*, Vol. 52, No. 15-16, pp. 6000-6011, (2009).

[9] A. Vali, C.J. Simonson, R.W. Besant, G. Mahmood, "Numerical model and effectiveness correlations for a run-around heat recovery system with combined counter and cross flow exchangers", *Int. J. Heat Mass Transf.*, Vol. 52, No. 25-26, pp. 5827-5840, (2009).

[10] S-M . Huang, L-Z. Zhang, K. Tang, L-X. Pei, "Fluid flow and heat mass transfer in membrane parallel-plates channels used for liquid desiccant air

dehumidification", *Int. J. Heat Mass Transf.*, Vol. 55, No. 9-10, pp. 2571-2580, (2012).

[11] D. Storle, M.R. Abdel-salam, N. Pourmahmoud, C.J. Simonson, "Performance Of The Dehumidification Cycle Of A 3-Fluid Liquid Desiccant Membrane Air-Conditioning System MSc". *Proc. of Building Simulation 15th Conference of IBPSA*, "*International building Performance Simulation Association*" San Francisco, CA, USA, pp. 2533–2539, (2017).

[12] M. Rashidzadeh, N. Pourmahmoud, and C.J. Simonson," 3D computational fluid dynamics simulation of a 3-fluid liquid-to-air membrane energy exchanger (LAMEE)", Appl. Therm. Eng., Vol. 153, No. pp. 501-512, (2019).

[13] A.E. Kabeel, Mofreh H. Hamed, Z.M. Omara, S.W. Sharshir, "Experimental study of a humidification-dehumidification solar technique by natural and forced air circulation", *Energy.*, Vol. 68, No. pp. 218-228, (2014).

[14] L-Z. Zhang, "Heat and mass transfer in a cross-flow membrane-based enthalpy exchanger under naturally formed boundary conditions", *Int. J. Heat Mass Transf.*, Vol. 50, No. 1-2, pp. 151-162, (2007).

[15] H. Jafarian, H. Sayyaadi, F. Torabi, "Numerical modeling and comparative study of different membrane-based liquid desiccant dehumidifiers", *Energy Convers. Manag.*, Vol. 184, No. pp. 735-747, (2019).

[16] J. Lin, S-M. Huang, R. Wang, K.J. Chua, "Thermodynamic analysis of a hybrid membrane liquid desiccant dehumidification and dew point evaporative cooling system", *Energy Convers. Manag.*, Vol. 156, No. pp. 440-458, (2018).

[17] M.R. Conde, "Properties of aqueous solutions of lithium and calcium chlorides: formulations for use in air conditioning equipment design", *Int. J. Heat Mass Transf.*, Vol. 43, No. 4, pp. 367-382, (2004).

[18] C. Simonson and R. Besant, "Energy wheel effectiveness: part I—development of dimensionless groups", *Int. J. Heat Mass Transf.*, Vol. 42, No. 12, pp. 2161-2170, (1999).

[19] M.R. Abdel-Salam, R.W. Besant, C.J. Simonson, "Performance Definitions for Three-Fluid Heat and Moisture Exchangers", *J Heat Transfer.*, Vol. 139, No. 2, pp. 022003-1-022003-8, (2017).

[20] S.M. Ghiaasiaan, *Convective heat and mass transfer*, 2nd ed., Cambridge University Press; (2018).

[21] H.B. Hemingson, C.J. Simonson, R.W. Besant, "Steady-state performance of a run-around membrane energy exchanger (RAMEE) for a range of outdoor air conditions", *Int. J. Heat Mass Transf.*, Vol. 54, No. 9-10, pp. 1814-1824, (2011).

[22] A. Vali, *Modeling a run-around heat and moisture exchanger using two counter/cross flow exchangers*, PhD thesis, (2009).

[23] M. Seyed Ahmadi, *Modeling the transient behavior of a run-around heat and moisture exchanger system*, PhD thesis, University of Saskatchewan, (2008).

[24] H. Sadighi Dizaji, S. Jafarmadar, M. Hashemian, "The effect of flow, thermodynamic and geometrical characteristics on exergy loss in shell and coiled tube heat exchangers", *Energy.*, Vol. 91, No., pp. 678-684, (2015).

[25] E.K. Akpinar, Y. Bicer, "Investigation of heat transfer and exergy loss in a concentric double pipe exchanger equipped with swirl generators", *Int. J. Therm. Sci.*, Vol. 44, No. 6, pp. 598-607, (2005).

[26] E.K. Akpinar, "Evaluation of heat transfer and exergy loss in a concentric double pipe exchanger equipped with helical wires", *Energy Convers. Manag.*, Vol. 47, No. 18-19, pp. 3473-3486,

(2006).